Effect of Layer Number and Crystal Stacking Orientation on the Raman Spectra of Two-Dimensional MoS_2

David Tuschel

The number of stoichiometric layers and crystal stacking orientation affect the Raman spectra of two-dimensional MoS_2 prepared by chemical vapor deposition on silicon substrates. Raman imaging in the low-energy region of the spectrum is used to reveal the spatial variation of the single, double, and triple trilayers in MoS_2. Crystals with different stacking orientation were analyzed by Raman spectroscopy. The low-energy shear and interlayer breathing modes' peak positions and signal strengths depend on the parallel or anti-parallel crystal stacking orientation as the number of trilayers increase. The progression of relative peak positions in a crystal with parallel trilayer orientation is the opposite of that observed for crystals with anti-parallel trilayer orientation.

We have discussed Raman spectroscopy and imaging of few-layer exfoliated MoS_2 low-energy phonons in a previous installment of "Molecular Spectroscopy Workbench" (1). These two-dimensional (2D) crystals are structures consisting of individual atomic layers of sulfur, molybdenum, and sulfur atoms corresponding to the stoichiometric unit of MoS_2. The plane of molybdenum atoms is sandwiched above and below by planes of sulfur atoms. Therefore, we describe each stoichiometric layer in a crystal of MoS_2 as a trilayer of sulfur, molybdenum, and sulfur atomic planes. In recent years, new inorganic 2D materials have emerged, including MoS_2, $MoSe_2$, WS_2, and WSe_2, among others. These materials have attracted significant interest because of special electronic, optical, and optoelectronic properties in the single trilayer to few-layer forms that are different from those manifest by the bulk form (2,3). One of the most important differences of the 2D crystals is the transformation from an indirect band gap semiconductor in the bulk, to a direct band gap semiconductor in the single trilayer, to few-layer crystals. Thus, the fabrication of optoelectronic devices in addition to familiar integrated electronic circuitry is envisioned for these materials. These optoelectronic characteristics have prompted substantial research to discover the means of fabrication and the physical characteristics of two-dimensional crystals to produce integrated electronic and optoelectronic devices (3).

There is a great need to characterize these materials and correlate the solid-state structure to their physical properties. The experimental nature of these materials leads to structural variability often within a single film. Consequently, there have been attempts to develop analytical methods for the reliable characterization of 2D crystals. You may have observed the spatially varying colors in reflected white light images of nanomaterials, and so there have been developments to use optical microscopy to rapidly identify the number of stoichiometric layers that make up the two-dimensional crystal (4). In this installment, we address the effect of trilayer number and crystal stacking orientation on the Raman spectra of 2D MoS_2 prepared by chemical vapor deposition (CVD) on silicon (Si) substrates with a thin silicon oxide (SiO_2) surface film.

Effect of Layer Number on Raman Spectra

A reflected white light image of MoS_2 single and double trilayer (TL) crystals, prepared by chemical vapor deposition on a Si substrate, is shown in Figure 1. The crystals form a triangular crystal habit consistent with the trigonal prismatic coordination of the Mo atoms and crystal structure of MoS_2, D_{3h} for odd, and D_{6h} for even numbers of trilayers, respectively. The light pink triangles consist of a single trilayer of MoS_2, whereas the darker colored features in the triangle interior consist of two trilayers. Raman spectra were acquired using 532 nm excitation from the light and dark pink areas, and are shown in Figure 2. The light pink, single trilayer spectrum consists of the substrate Si band at 520 cm^{-1}, and the E^1_{2g} and A_{1g} bands of MoS_2 at 383.5 and 403.5 cm^{-1}, respectively. The absence of low-energy bands in the region below 50 cm^{-1} indicates that the light pink triangles consist of a single trilayer; that is, there can be no low-energy shear or interlayer breathing modes where only one trilayer exists. A darker pink structure seen in the center of the MoS_2 triangle in Figure 1 consists of two trilayers, a spectrum from which is also shown in Figure 2. The dark pink region spectrum consists of the Si substrate band and the E^1_{2g} and A_{1g} bands of MoS_2 at 382.5 and 405.5 cm^{-1}, as well as bands at 22.0 and 39.5 cm^{-1} assigned to E^2_{2g} and the B^2_{2g} , respectively. Note the increase of the signal strength of the E^1_{2g} and A_{1g} bands of MoS_2 at 382.5 and 405.5 cm^{-1} relative to that of the substrate Si band in the spectrum from the dark pink region compared to that of the light pink area. The stronger signal from the MoS_2 bands in the dark pink region is consistent with a greater number of trilayers. Furthermore, the increase in separation of the E^1_{2g} and A_{1g} bands of MoS_2 from 20.0 cm^{-1} in the spectrum from the light pink area to 23.0 cm^{-1} in that from the dark pink region supports an assignment of these areas as single and double trilayers, respectively.

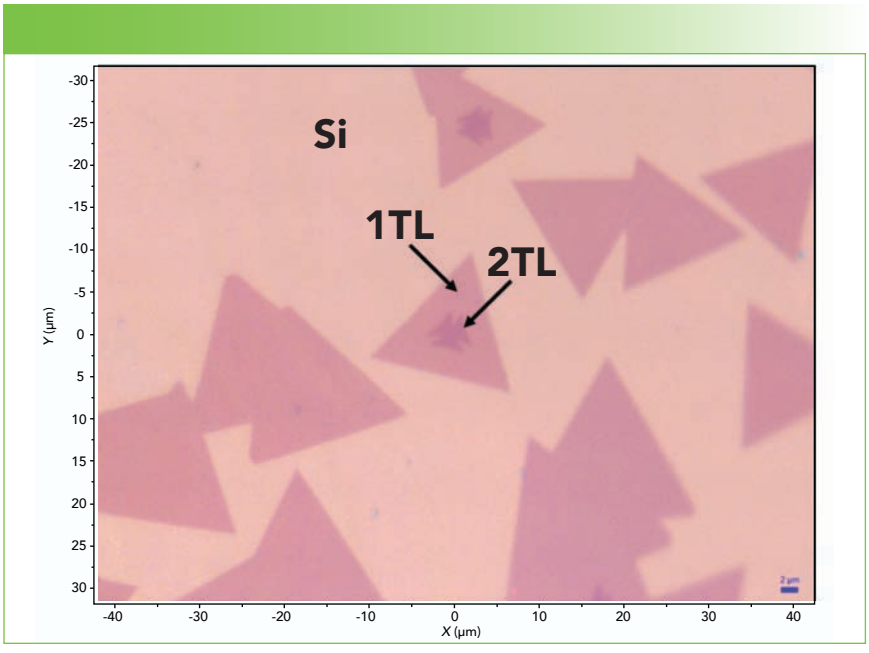

FIGURE 1: Reflected white light image of MoS_2 with single (1TL) and double (2TL) trilayers prepared by chemical vapor deposition on a Si substrate.

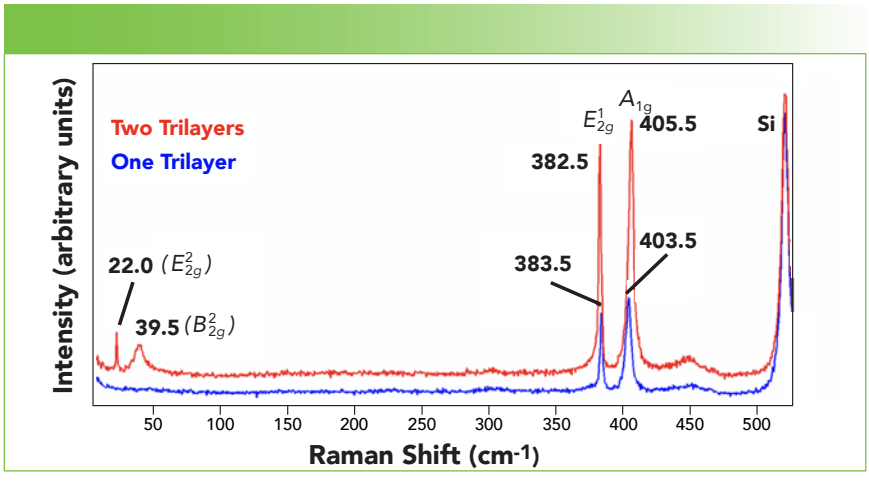

FIGURE 2: Raman spectra acquired from the light pink (blue spectrum) and dark pink (red spectrum) areas shown in Figure 1.

Here, we address our assignment of the low-energy Raman bands, and do so following the work of Zhang and coworkers on shear and interlayer breathing modes of MoS_2 (5). The crystals with odd numbers of trilayers belong to crystal class D_{3h}, whereas those with even numbers of trilayers belong to D_{6h}. The Zhang calculations, based on a diatomic chain model (DCM), predict a Raman active E^2_{2g} mode at 23 cm^{-1}, and a silent B^2_{2g} mode at 40 cm^{-1} for a 2D MoS_2 crystal consisting of two trilayers. Although the B^2_{2g} mode is silent, Zhang and coworkers state that "the Raman inactive layer breathing modes (LBMs) (B^2_{2g}) in even number layered MoS_2 might be observed, with polarization behavior identical to the A'_1 (LBMs) in odd number

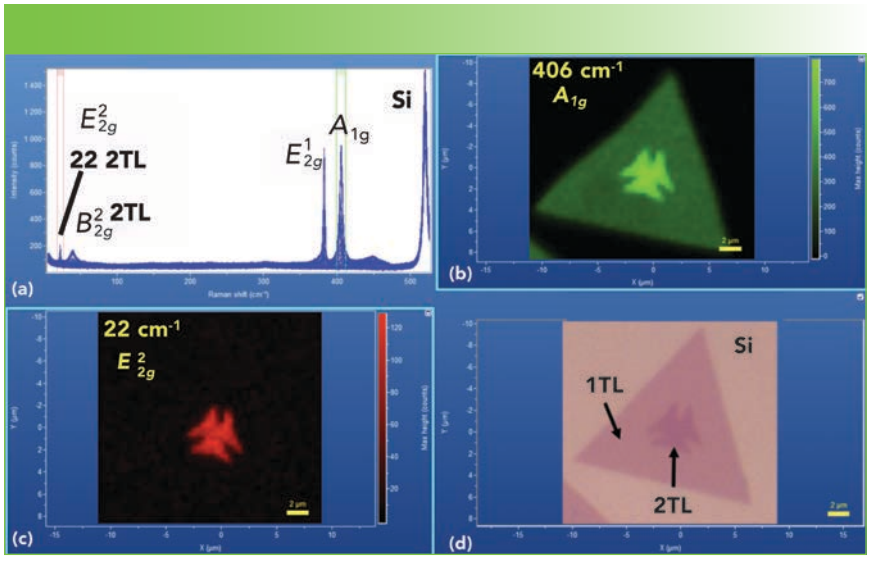

FIGURE 3: (a) Raman spectra and images acquired from the (b) single (1TL) and (c) double (2TL) trilayer areas as shown in (d) and in Figure 1.

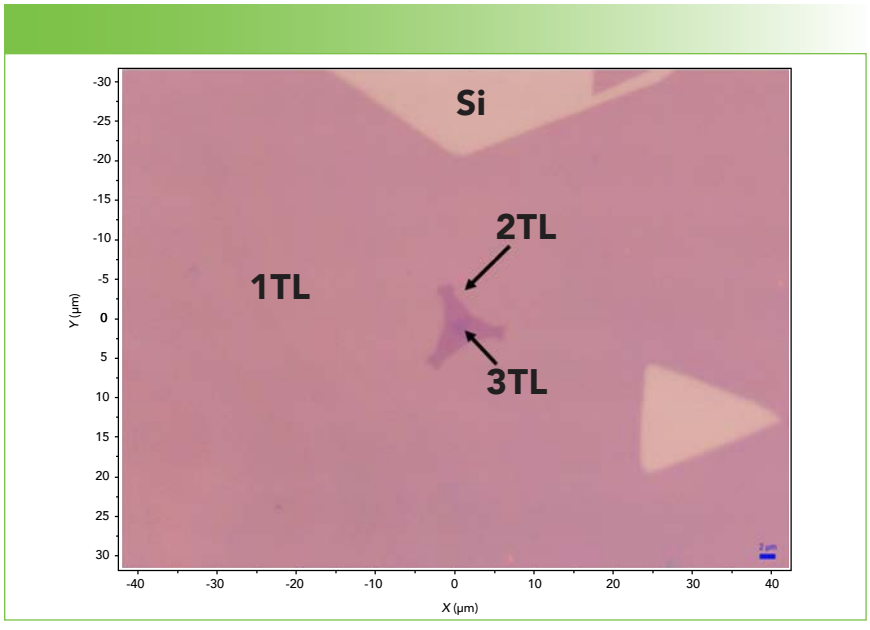

FIGURE 4: Reflected white light image of 2D MoS_2 with single (1TL), double (2TL) and triple (3TL) trilayers prepared by chemical vapor deposition on a Si substrate.

layered MoS_2" (5). Therefore, based on the appearance of bands at 22.0 cm^{-1} and 39.5 cm^{-1} in the spectrum of the dark pink region, in agreement with those calculated by Zhang and coworkers for the double trilayer crystal, we assign them to E^2_{2g} and B^2_{2g}, respectively. The absence and appearance of these low-energy bands, along with the increasing separation between the E^1_{2g} and A_{1g} bands of MoS_2 from 20.0 cm^{-1} to 23.0 cm^{-1} in the spectra of light and dark pink regions, is consistent with the Zhang calculations for single and double trilayers, respectively.

Raman imaging further supports the layer number assignment of the light and dark pink regions. A collection of hyperspectral data and corresponding Raman images acquired from the central 2D MoS_2 crystal of Figure 1 are shown in Figure 3. A reflected white light image of the crystal appears in the lower right hand corner, and corresponding 406 cm^{-1} (A_{1g}) and 22 cm^{-1} (E^2_{2g}) Raman images appear above and to the left of the reflected light image, respectively. The plot on the upper left consists of all of the Raman spectra acquired over the image area. The Raman data were acquired using 532 nm excitation and a 100X Olympus objective, and by moving the stage in 400 nm increments over an area of approximately 19 µm x 19 µm. The Raman images are rendered from the spatial variation of the Raman intensity within the color coded brackets shown in the hyperspectral data set in the upper left hand corner. The red and green brackets are centered on 22 cm^{-1} and 406 cm^{-1}, respectively. The differences in the signal strengths related to the number of trilayers can be clearly seen in the Raman image of the 406 cm^{-1} (A_{1g}) band shown in Figure 3. That portion of the 406 cm^{-1} (A_{1g}) band Raman image corresponding to the dark pink region is approximately twice as bright as the surrounding triangle of MoS_2. The association of that increased signal strength with the double trilayer is confirmed by the correspondence to, and registration with, the Raman image rendered from the mapping of the interlayer shear mode E^2_{2g} band signal strength at 22 cm^{-1}.

Crystals with three trilayers exhibit the same optical and spectral trends observed in progressing from a single to a double trilayer. A reflected white light image consisting of the Si substrate and 2D MoS_2, with single (1TL), double (2TL) and triple (3TL) trilayers, is shown in Figure 4. The single trilayer MoS_2 appears light pink, and the double and triple trilayers appear progressively darker. The dark triangle in the center of the image is a triple trilayer.

TABLE I: Comparison of experimentally obtained (exp) low-energy Raman band positions of double (2TL) and triple (3TL) trilayer crystals of MoS_2 with those calculated, based upon the diatomic chain model (DCM) of Zhang and coworkers (5).

Trilayers	E^2_{2g} (exp)	E^2_{2g} (DCM)	B^2_{2g} (exp)	B^2_{2g} (DCM)	E'' (exp)	E'' (DCM)	A'_1 (exp)	A'_1 (DCM)
1	-	-	-	-	-	-	-	-
2	22.0 cm^{-1}	23 cm^{-1}	39.5 cm^{-1}	40 cm^{-1}				
3					16.0 cm^{-1}	16 cm^{-1}	27.0 cm^{-1}	28 cm^{-1}

Raman spectra acquired from the areas with one, two, and three trilayers are shown in Figure 5. The single trilayer spectrum consists of the Si substrate Raman band and only the E^1_{2g} and A_{1g} bands at higher energy. The absence of the low-energy E^2_{2g} and B^2_{2g} bands confirms that the crystal in that location consists of only a single trilayer. The Raman spectrum from the double trilayer region consists of the Si substrate Raman band, the high-energy E^1_{2g} and A_{1g} bands, and two low-energy bands which we attribute to the shear (E^2_{2g}) and interlayer breathing modes (B^2_{2g}). The spectrum obtained from the triple trilayer triangle in the center of Figure 4 consists of the four bands that appear in the double trilayer spectrum. However, both low-energy bands are noticeably shifted to lower energy, and are assigned new symmetry species E'' and A'_1 commensurate with the change to the D_{3h} crystal class for odd trilayer MoS_2. These same spectra are plotted on an expanded scale in Figure 6. The E^1_{2g} and A_{1g} bands at higher energy manifest increasing band separation with trilayer number progressing from 20.5 cm^{-1} to 23.5 cm^{-1} to 25.0 cm^{-1} for the single, double, and triple trilayers, respectively.

The inset of the plot in Figure 6 shows an expanded scale of the low-energy region of the spectrum. The double trilayer spectrum with bands at 22.5 cm^{-1} and 39.5 cm^{-1} is in good agreement with that shown in Figure 2. The triple trilayer spectrum has low-energy bands; however, they have shifted to 16.0 cm^{-1} and 27.0 cm^{-1}, respectively. These experimental results are in good agreement with those values calculated based upon the diatomic chain model (DCM) (5). The experimentally obtained results along with the DCM expectations calculated by Zhang and coworkers are shown in Table I.

In summary, we can conclude that the low-energy band positions are consistent with and provide the same information regarding the number of trilayers as does the higher

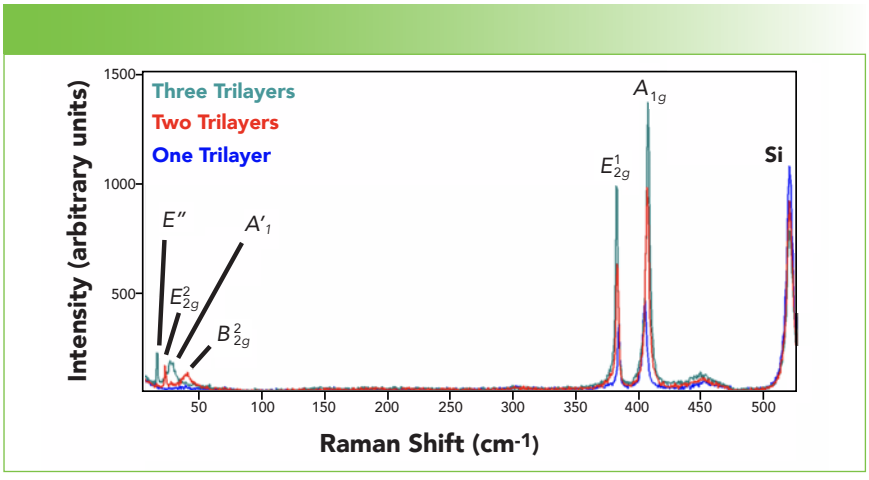

FIGURE 5: Raman spectra acquired from the single (blue), double (red) and triple (green) trilayer areas shown in Figure 4.

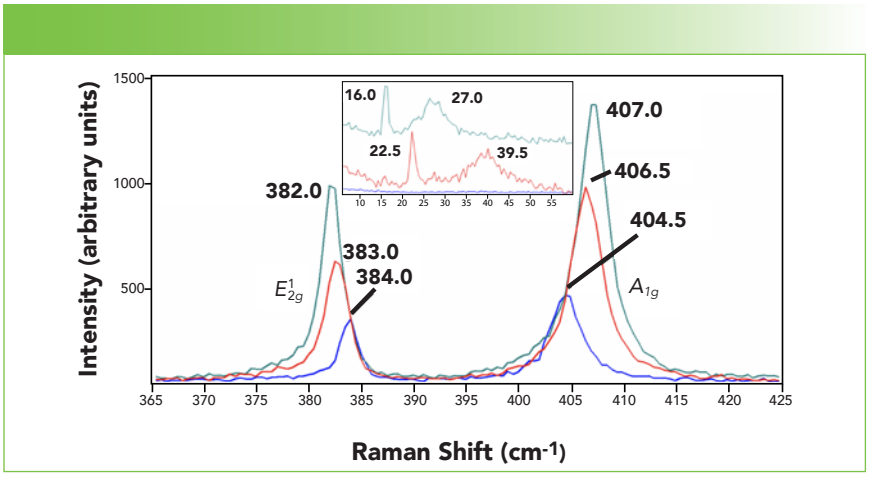

FIGURE 6: Raman spectra acquired from the single (blue), double (red) and triple (green) trilayer areas as shown in Figure 4.

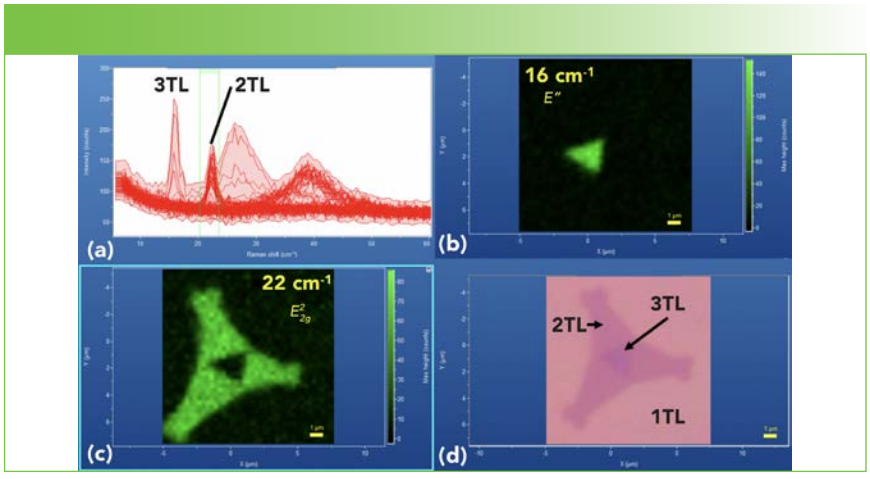

FIGURE 7: (a) Raman spectra and images acquired from single, (c) double (2TL at 22 cm^{-1}), and (b) triple (3TL at 16 cm^{-1}) trilayer areas as shown (d) and in Figure 4.

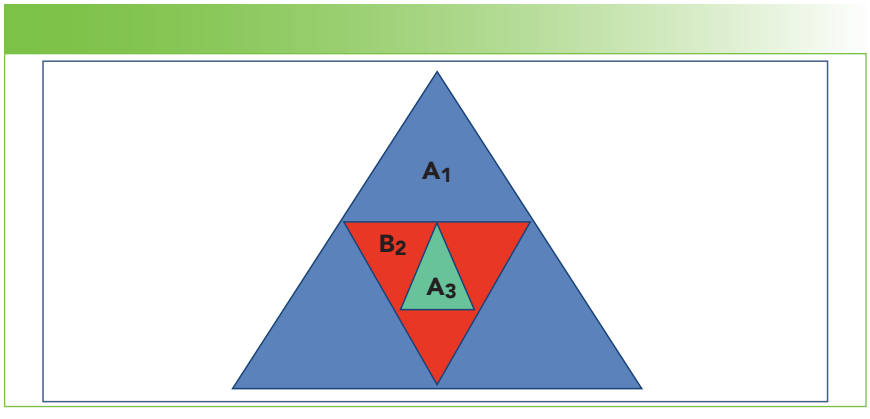

FIGURE 8: Labeling system and graphic of 2D Si substrate crystal few-layer orientation. The graphic depicts a three trilayer crystal of order and orientation $A_1B_2A_3$, where the first large blue A_1 is on the Si substrate, the red B_2 is on top of blue A_1, and the green A_3 is on top of red B_2.

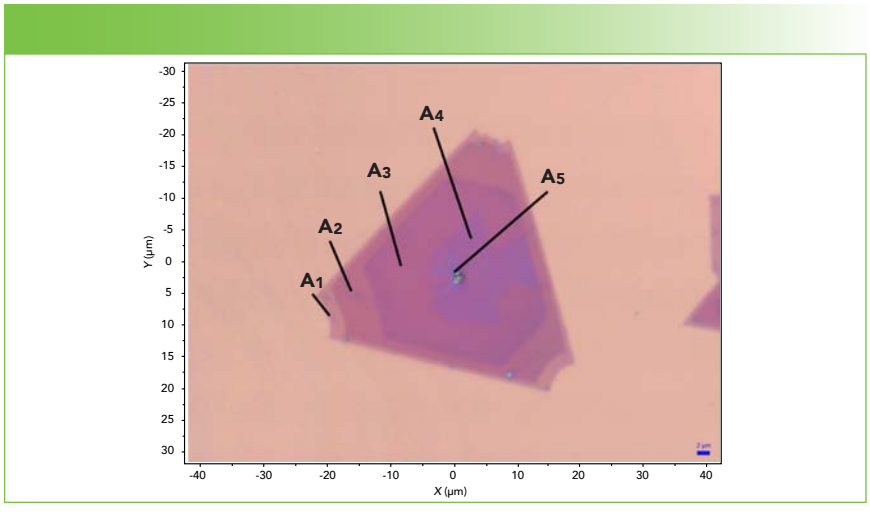

FIGURE 9: Reflected white light image of a five trilayer $A_1A_2A_3A_4A_5$ oriented 2D MoS_2 crystal prepared by chemical vapor deposition on a Si substrate.

energy E^1_{2g} and A_{1g} band separation for few-layer MoS_2. Nevertheless, the low-energy band positions change to a greater extent than does the higher energy E^1_{2g} and A_{1g} band separation and are therefore more sensitive to the number of trilayers in 2D MoS_2.

The distinction between the double and triple trilayers and correspondence to the reflected white light image can be seen in the 22 cm^{-1} and 16 cm^{-1} Raman images shown in Figure 7. A reflected white light image of the crystal appears in the lower right hand corner and corresponding 16 cm^{-1} (E'') and 22 cm^{-1} (E^2_{2g}) Raman images appear above and to the left of the reflected light image, respectively. The plot on the upper left consists of all of the Raman spectra acquired over the image area. The Raman data were acquired using 532 nm excitation and a 100X Olympus objective and by moving the stage in 300 nm increments over an area of approximately 13 µm x 13 µm. The 22 cm^{-1} band intensity attributed to the double trilayer is appreciable only in the three-pronged structure and is absent in the single and triple trilayer areas. The 16 cm^{-1} band appears only in the triangle at the center, the triple trilayer. These images demonstrate how Raman imaging in the low-energy region of the spectrum can readily be used to reveal the spatial variation of the single, double and triple trilayers in MoS_2.

Crystal Stacking Orientation and Low-Energy Band Position

The interpretation of the Raman spectra in the low-frequency region is made complex by the different symmetry species of the low-energy vibrational modes for odd and even numbers of trilayers (5–9). Furthermore, other reports have shown how stacking orientation can affect interlayer coupling and therefore the positions of the low-energy bands arising from shear and interlayer breathing modes (10–12). We discuss here how the progression of the shear and interlayer breathing modes' peak positions and signal strengths depend upon the parallel

or anti-parallel layer orientation as the number of trilayers increase.

To facilitate the discussion of spectra obtained from 2D crystals of MoS_2 with parallel or anti-parallel stacking of crystal layers, we use the labeling system described in Figure 8. The graphic depicts a three trilayer crystal of order and orientation $A_1B_2A_3$. The first trilayer (1) on the substrate is pointed upwards (A) and so we designate that trilayer A_1. If the second trilayer (2) on top of the first trilayer is pointed downwards (B), we designate that trilayer B_2. A third trilayer (3) on top of the second trilayer that is pointed upwards is designated A_3, and so on.

A reflected white light image of a five trilayer $A_1A_2A_3A_4A_5$ oriented 2D MoS_2 crystal on a Si substrate is shown in Figure 9. Raman spectra obtained from an exposed portion of each level of the trilayers are shown in Figure 10. The intensity scale of the spectra in Figure 10 has been set to more clearly view the progressive shift of the low-energy shear mode (SM) and interlayer breathing mode (BM) bands to lower wavenumbers with increasing trilayer number. Although one cannot see it in Figure 10, the higher energy E^1_{2g} and A_{1g} band separation increases with each additional trilayer (17.7 cm^{-1} [A_1], 21.5 cm^{-1} [A_2], 25.5 cm^{-1} [A_3], 25.7 cm^{-1} [A_4], and 25.9 cm^{-1} [A_5]). This band separation is commonly used to determine the number of trilayers in the 2D crystal. However, we see again that the low-energy shear mode and interlayer breathing mode band positions are more sensitive to the number of trilayers, particularly beyond three trilayers. An expanded scale plot of these same spectra is shown in Figure 11 wherein the low-energy peak positions are labeled. Note that both the shear and interlayer breathing modes move progressively to lower energy with increasing trilayer number. Furthermore, the intensities of the shear and interlayer breathing modes remain fairly constant relative to those of the higher energy E^1_{2g} and A_{1g} bands. Therefore, we can conclude that the interlayer bond po-

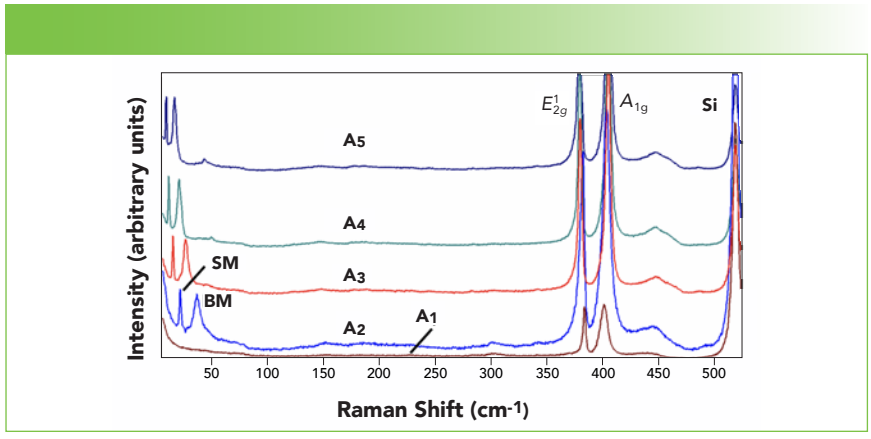

FIGURE 10: Raman spectra highlighting the shear mode (SM) and interlayer breathing mode (BM) of one (A_1), two (A_2), three (A_3), four (A_4) and five (A_5) trilayer locations in the $A_1A_2A_3A_4A_5$ oriented 2D MoS_2 crystal shown in Figure 9.

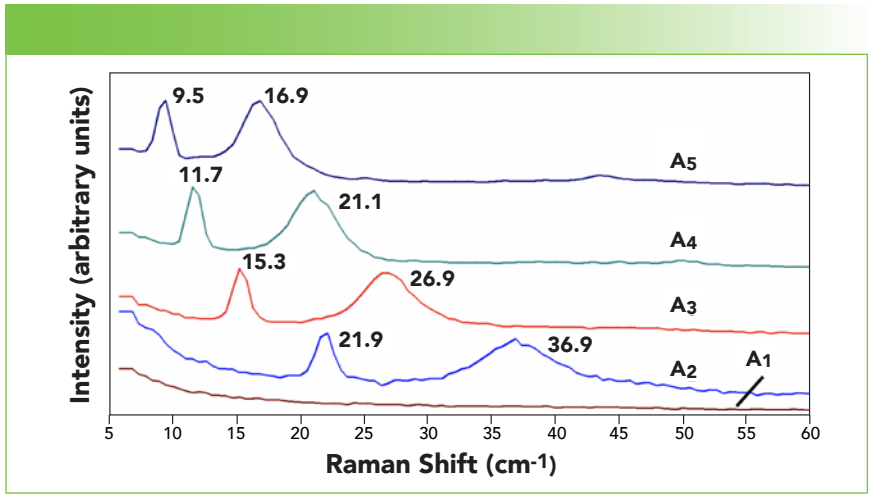

FIGURE 11: Raman spectra highlighting the shear mode and interlayer breathing mode shifts of one (A_1), two (A_2), three (A_3), four (A_4) and five (A_5) trilayer locations in the $A_1A_2A_3A_4A_5$ oriented 2D MoS_2 crystal shown in Figure 9.

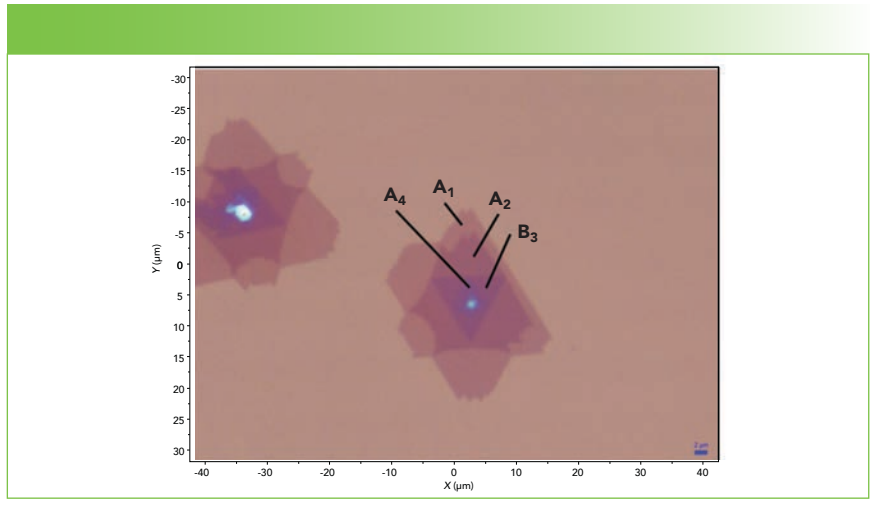

FIGURE 12: Reflected white light image of a four trilayer $A_1A_2B_3A_4$ oriented 2D MoS_2 crystal prepared by chemical vapor deposition on a Si substrate.

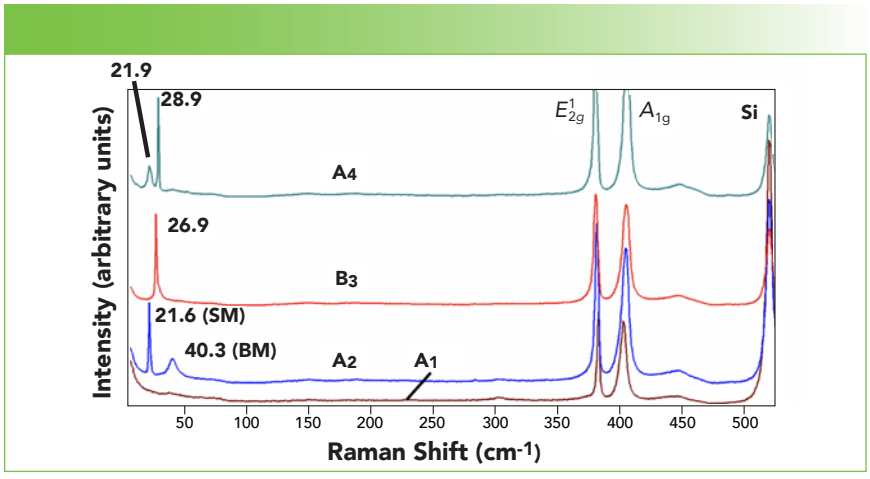

FIGURE 13: Raman spectra highlighting the shear mode (SM) and interlayer breathing mode (BM) of one (A_1), two (A_2), three (B_3), and four (A_4) trilayer locations in the $A_1A_2B_3A_4$ oriented 2D MoS_2 crystal shown in Figure 12.

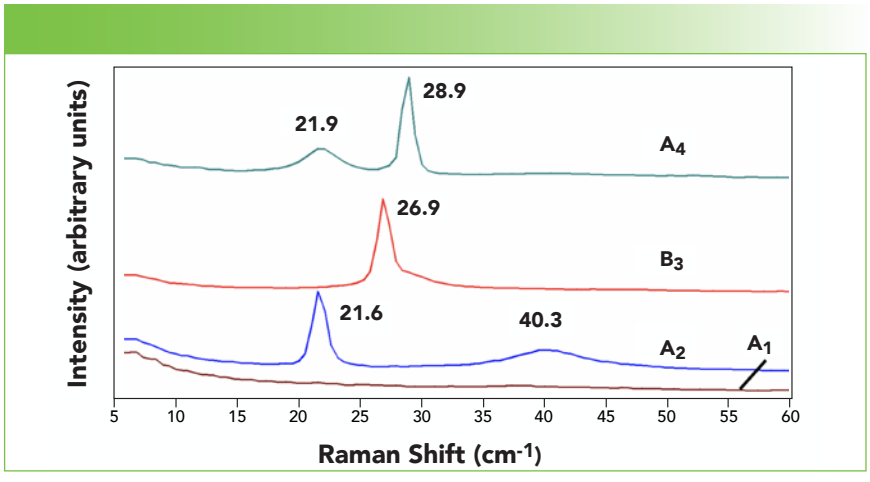

FIGURE 14: Raman spectra highlighting the shear mode and interlayer breathing mode shifts of one (A_1), two (A_2), three (B_3), and four (A_4) trilayer locations in the $A_1A_2B_3A_4$ oriented 2D MoS_2 crystal shown in Figure 12.

larizabilities do not substantially increase with increasing trilayer number in the $A_1A_2A_3A_4A_5$ parallel oriented 2D MoS_2.

An anti-parallel alignment of successive trilayers in oriented 2D MoS_2 yields a markedly different progression of the peak positions of the low-energy bands with increasing number of trilayers. A reflected white light image of a four trilayer $A_1A_2B_3A_4$ oriented 2D MoS_2 crystal is shown in Figure 12. Raman spectra obtained from an exposed portion of each level of the trilayers are shown in Figure 13. Note how much more intense the shear mode band (21.6 cm^{-1} in A_2) is in the spectra of the anti-parallel $A_1A_2B_3A_4$ oriented form of the 2D MoS_2 crystal compared to its counterpart in the $A_1A_2A_3A_4A_5$ parallel oriented crystal spectra as seen in Figure 10. Furthermore, the strength of the shear mode in the third anti-parallel trilayer (26.9 cm^{-1} in B_3) of the $A_1A_2B_3A_4$ oriented MoS_2 spectrum is comparable to those of the higher energy E^1_{2g} and A_{1g} bands in the same spectrum. The increased signal strength of the shear mode band indicates an increase in the interlayer polarizability when the trilayers are oriented anti-parallel with respect to each other. An expanded scale plot of these same spectra is shown in Figure 14 to more clearly see the shifts in the opposite directions of the shear and interlayer breathing mode bands with increasing trilayer number. The peak positions of the two trilayer (A_2) shear and interlayer breathing modes at 21.6 cm^{-1} and 40.3 cm^{-1} in the $A_1A_2B_3A_4$ oriented crystal spectrum are similar to those of the $A_1A_2A_3A_4A_5$ orientation at 21.9 cm^{-1} and 36.9 cm^{-1} shown in Figures 14 and 11, respectively. However, the presence of a third trilayer oriented anti-parallel with respect to the first two trilayers in the $A_1A_2B_3A_4$ oriented crystal causes the shear mode to shift from 21.6 cm^{-1} (A_2) to a higher energy at 26.9 cm^{-1} (B_3), whereas the interlayer breathing mode shifts to lower energy just as it does in the $A_1A_2A_3A_4A_5$ orientation. In fact, because the shear and interlayer breathing mode bands shift in the opposite direction with anti-parallel orientation, they are now closely spaced and only partially resolved in trilayer B_3. The effect of the third layer anti-parallel orientation on the directional shifts of the low-energy bands continues with the fourth trilayer (A_4) even though it has the same orientation as that of the first two layers. The shear and interlayer breathing mode peak positions of the fourth trilayer (A_4) are 28.9 cm^{-1} and 21.9 cm^{-1}, respectively. The relative positions of the shear and interlayer breathing mode bands in the $A_1A_2B_3A_4$ oriented crystal spectrum have reversed in progressing from trilayer levels A_2 to A_4. The principal finding is that the progression of relative peak positions of the shear and interlayer breathing modes in a crystal with anti-parallel trilayer orientation is the opposite of that observed for crystals with parallel trilayer orientation.

It is important to note that the effects of trilayer orientation extend throughout the 2D crystal, including exposed perimeters of underlying trilayers. Compare the relative signal strengths of the shear and interlayer breathing modes of the two trilayer spectra (A_2) in the $A_1A_2A_3A_4A_5$ and $A_1A_2B_3A_4$ crystals. Measured at a location at which only the first two trilayers are exposed, one might suppose that the spectra would be the same were

the material to be simply a collection of MoS_2 trilayers, and not a 2D crystal. The band positions are indeed similar; however, the Raman signal strength of the A_2 shear mode band in the $A_1A_2B_3A_4$ crystal spectrum is significantly greater than its counterpart band in the spectrum of the $A_1A_2A_3A_4A_5$ crystal. This spectral behavior confirms that the entire material is indeed a 2D crystal with interlayer forces extending beyond trilayer perimeters to exposed levels below.

The spectral results discussed here have important consequences for the characterization of continuous 2D films with no obvious crystal habit revealing the solid-state structure. The combination of reflected white light images with the corresponding Raman spectra of exposed levels can be used to establish reference spectra of the number and stacking orientation of trilayers in 2D MoS_2 crystals. The reference low-energy Raman band structure can then reveal the number and orientation of the trilayers in 2D MoS_2 even when the reflected white light image of a crystal or extended film may not reveal the number of trilayers or stacking orientation.

Conclusion

We acquired and analyzed Raman spectra of few-layer 2D MoS_2 crystals prepared by chemical vapor deposition and consisting of different numbers of trilayers. We observed that the low-energy band positions change to a greater extent than does the separation of higher energy E^1_{2g} and A_{1g} bands and are therefore more sensitive to the number of trilayers in 2D MoS_2. Raman imaging was performed on these crystals and demonstrated how Raman images of the low-energy region of the spectrum reveal the spatial variation of the single, double and triple trilayers in MoS_2. Crystals consisting of different stacking orientation were analyzed by Raman spectroscopy. The shear and interlayer breathing modes' peak positions and signal strengths depend upon the parallel or anti-parallel crystal stacking orientation as the number of trilayers increase. The principal finding is that the progression of relative peak positions of the shear and interlayer breathing modes in a crystal with anti-parallel trilayer orientation is the opposite of that observed for crystals with parallel trilayer orientation.

References

(1) D. Tuschel, *Spectroscopy* **30**(9), 18–31 (2015).

(2) D. Jariwala, V.K. Sangwan, L.J Lauhon, T.J. Marks, and M.C. Hersam, *ACS Nano* **8**, 1102–1120 (2014).

(3) G. Eda and S.A. Maier, *ACS Nano* **7**, 5660–5665 (2013).

(4) H. Li, J. Wu, X. Huang, G. Lu, J. Yang, X. Lu, Q. Xiong, and H. Zhang, ACS Nano **7**, 10344–10353 (2013).

(5) X. Zhang, W.P. Han, J.B. Wu, S. Milana, Y. Lu, Q.Q. Li, A.C. Ferrari, and P.H. Tan, *Phys. Rev. B* **87**, 115413 (2013).

(6) H. Zeng, B. Zhu, K. Liu, J. Fan, X. Cui, and Q.M. Zhang, *Phys. Rev. B* **86**, 241301(R) (2012).

(7) L. Liang, J. Zhang, B.G. Sumpter, Q.-H. Tan, P.-H. Tan, and V. Meunier, *ACS Nano* **11**, 11777–11802 (2017).

(8) X. Zhang, X.-F. Qiao, W. Shi, J.-B. Wu, D.-S. Jiang, and P.-H. Tan, *Chem. Soc. Rev.* **44**, 2757–2785 (2015).

(9) Y. Zhao, X. Luo, H. Li, J. Zhang, P.T. Araujo, C.K. Gan, J. Wu, H. Zhang, S.Y. Quek, M.S. Dresselhaus, and Q. Xiong, *Nano Lett.* **13**, 1007–1015 (2013).

(10) J. Yan, J. Xia, X. Wang, L. Liu, J.-L. Kuo, B.K. Tay, S. Chen, W. Zhou, Z. Liu, and Z.X. Shen, *Nano Lett.* **15**, 8155–8161 (2015).

(11) M. O'Brien, N. McEvoy, D. Hanlon, T. Hallam, J.N. Coleman, and G.S. Duesberg, *Sci. Reports* **6**, 19476 (2016).

(12) X. Luo, X. Lu, C. Cong, T. Yu, Q. Xiong, and S.Y. Quek, *Sci. Reports* **5**, 14565 (2015).

David Tuschel is a Raman applications scientist at Horiba Scientific, in Piscataway, New Jersey, where he works with Fran Adar. David is sharing authorship of this column with Fran. He can be reached at: SpectroscopyEdit@MMHGroup.com